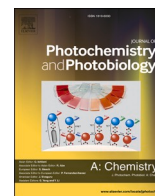




Contents lists available at ScienceDirect

Journal of Photochemistry &amp; Photobiology, A: Chemistry

journal homepage: [www.elsevier.com/locate/jphotochem](http://www.elsevier.com/locate/jphotochem)

## The synergy of CHEF and ICT toward fluorescence ‘turn-on’ probes based on push-pull benzothiazoles for selective detection of Cu<sup>2+</sup> in acetonitrile/water mixture

Jukkrit Nootem<sup>a</sup>, Rathawat Daengngern<sup>b</sup>, Chanchai Sattayanon<sup>g</sup>, Worawat Wattanathana<sup>c</sup>, Suttipong Wannapaiboon<sup>d</sup>, Paitoon Rashatasakhon<sup>e,f</sup>, Kantapat Chansaenpak<sup>a,f,\*</sup>

<sup>a</sup> National Nanotechnology Center, National Science and Technology Development Agency, Thailand Science Park, Pathum Thani, 12120, Thailand

<sup>b</sup> Integrated Applied Chemistry Research Unit, School of Science, King Mongkut's Institute of Technology Ladkrabang, Bangkok, 10520, Thailand

<sup>c</sup> Department of Materials Engineering, Faculty of Engineering, Kasetsart University, Ladyao, Chatuchak, Bangkok, 10900, Thailand

<sup>d</sup> Synchrotron Light Research Institute, 111 University Avenue, Suranaree, Muang, Nakhon, Ratchasima, 30000, Thailand

<sup>e</sup> Department of Chemistry, Faculty of Science, Chulalongkorn University, Bangkok, 10330, Thailand

<sup>f</sup> Research Network of Nanotec-CU on Nanotechnology for Food and Agriculture, Department of Chemistry, Faculty of Science, Chulalongkorn University, Bangkok, 10330, Thailand

<sup>g</sup> School of Liberal Arts, King Mongkut's University of Technology Thonburi, Bangkok, 10140, Thailand

### ARTICLE INFO

**Keywords:**  
Fluorescence  
Sensor  
Copper  
Benzothiazole  
Drinking water

### ABSTRACT

New push-pull schiff base ligands based on benzothiazole (BZ) unit were developed for the selective detection of Cu<sup>2+</sup> through fluorescence ‘turn-on’ mechanism. These derivatives with electron withdrawing trifluoromethyl (-CF<sub>3</sub>) and cyano (-CN) substituents (BZ2 and BZ3) demonstrated a prominent fluorescence enhancement upon copper ion binding which could be the results from the synergistic effect between the chelation-enhanced fluorescence (CHEF) and the intramolecular charge transfer (ICT) processes. In addition, these compounds displayed 1:1 binding with Cu<sup>2+</sup> with low limits of detection of 0.77 μM and 0.64 μM for BZ2 and BZ3, respectively, in acetonitrile-water (3:1 v/v) media. The electronic and photophysical properties of these BZ ligands and the copper ion complexes were modelled by the density functional theory (DFT) and the time-dependent density functional theory (TD-DFT) calculations, respectively. Analysis of X-ray absorption spectra probed at Cu K-edge of Cu<sup>2+</sup>-BZ mixtures revealed the complex formation of BZ ligands with the targeted Cu<sup>2+</sup> and confirmed the non-centrosymmetric structures of the complexes as predicted by the DFT calculation. The electron density distributions of the HOMO-LUMOs in the computational results as well as large stokes shifts of the ligand-metal complexes in the experimental data confirmed the strong ICT effect after Cu<sup>2+</sup> binding which is a key process promoting fluorescence ‘turn-on’ mechanism.

### 1. Introduction

Copper ion (Cu<sup>2+</sup>) is the third most abundant transition metal ion in human body after ferrous (Fe<sup>2+</sup>) and zinc (Zn<sup>2+</sup>) ions, respectively [1]. It plays essential roles in several biological processes, such as a cofactor for electron transfers in many proteins or a catalyst for redox reactions in biological pathways. However, excessive uptake of copper ions in human can cause severe neurodegenerative diseases, including, Alzheimer, Parkinson, Huntington and Prion diseases [2]. In addition, long-term exposure to copper ion can give rise to liver or kidney damage

as well as gastrointestinal disturbance [3,4]. Due to these detrimental effects to human health, fluorescent sensors for Cu<sup>2+</sup> have gained much attention and a number of them have been developed to detect copper contaminants in environments, waters, and cellular matrices [5–8].

Cu<sup>2+</sup> ion is well known as a fluorescence quencher due to its paramagnetic effect, so that, most of fluorescent chemosensors detected Cu<sup>2+</sup> via fluorescence quenching processes. [9–14] However, chemosensors possessing fluorescence enhancement are more desirable as they can be simply monitored and more applicable for biological studies, such as, cellular or small animal imaging [7,15,16]. The fluorescence turn-on

\* Corresponding author at: National Nanotechnology Center, National Science and Technology Development Agency, Thailand Science Park, Pathum Thani, 12120, Thailand.

E-mail address: [kantapat.cha@nanotec.or.th](mailto:kantapat.cha@nanotec.or.th) (K. Chansaenpak).

<https://doi.org/10.1016/j.jphotochem.2021.113318>

Received 26 January 2021; Received in revised form 3 April 2021; Accepted 21 April 2021

Available online 25 April 2021

1010-6030/© 2021 Elsevier B.V. All rights reserved.

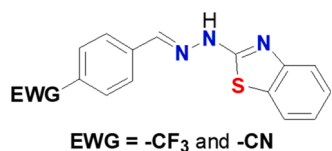


Fig. 1. The proposed push-pull benzothiazole molecules in this work.

probes can be constructed based on various mechanisms, such as, chelation-induced enhanced fluorescence (CHEF) [17], intramolecular charge transfer (ICT) [18], excited-state intramolecular proton transfer (ESIPT) [19], and fluorescence resonance energy transfer (FRET) [20]. Among these, CHEF plays a vital role in metal sensing as most metal ions tend to chelate with the organic donor ligands. Indeed, CHEF phenomenon leads to an increased conjugation in organic molecule upon metal binding which could facilitate ICT process throughout the pi-systems yielding fluorescence enhancement [21]. However, the fluorescence probes relying on the synergy of CHEF and ICT are scarcely reported in literature, therefore, there is still a large room for improvement.

As part of our investigations on fluorescent sensors, we pinned our interest to the benzothiazole (BZ) backbone due to its ease of preparation and functionalization as well as its intrinsic optical properties. [22–30] Similar to other fluorescence sensors, most of benzothiazole derivatives detected Cu<sup>2+</sup> through fluorescence turn-off processes. [3, 31–35] Only a few examples can sense Cu<sup>2+</sup> via fluorescence turn-on pathway. [36] In this work, we have prepared novel push-pull benzothiazole derivatives employing a thiazole unit as an electron donor group and electron-withdrawing (EWG) functionalized phenylene as an electron acceptor moiety to acquire ICT effect (Fig. 1). The two nitrogen atoms in the proposed molecules are aimed to chelate Cu<sup>2+</sup> ion leading to fluorescence enhancement via CHEF and ICT processes. The experimental details as well as density functional theory (DFT) calculation results regarding Cu<sup>2+</sup> sensing were presented in this report.

## 2. Experimental section

### 2.1. Materials and instruments

2-Hydrazinobenzothiazole, benzaldehyde, 4-(trifluoromethyl)benzaldehyde, 4-formylbenzotrile, 4-(diethylamino)benzaldehyde, and glacial acetic acid were purchased from TCI Chemicals; all metal nitrate salts were purchased from Sigma Aldrich; ethanol (ACS grade) were purchased from Honeywell. Standard buffer solutions pH 1–12 were purchased from Merck (glycine/NaCl/HCl for pH 1, Citric acid/NaOH/HCl for pH 2–6, Na<sub>2</sub>HPO<sub>4</sub>/KH<sub>2</sub>PO<sub>4</sub> for pH 7, boric acid/ KCl/NaOH for pH 8–11, Na<sub>3</sub>PO<sub>4</sub>/NaOH for pH 12). All chemicals were used without further purification. Electrospray mass spectra were obtained from a Bruker microTOF spectrometer. NMR spectra were recorded on a Bruker NMR 400 and 500 MHz spectrometer at ambient temperature. Chemical shifts are given in ppm, and are referenced to residual <sup>1</sup>H and <sup>13</sup>C solvent signals. The crystallographic measurement was performed using a Bruker APEX-II CCD area detector diffractometer. UV–vis absorption and fluorescence spectra were acquired from a Cary Series UV–vis-NIR spectrophotometer (Agilent Tech, Santa Clara, CA, USA) and a Perkin Elmer LS55 fluorescence spectrometer, respectively.

### 2.2. General details for UV–vis and fluorescence measurements

#### 2.2.1. Preparation of the stock solutions

The stock solutions of BZ compounds was prepared by dissolving 30 mg of BZ with 50 mL of acetonitrile : water (3 : 1) solution in standard volumetric flasks (~ 2 mM). The stock solution of Cu(NO<sub>3</sub>)<sub>2</sub>·3H<sub>2</sub>O was prepared by dissolving 30 mg of Cu(NO<sub>3</sub>)<sub>2</sub>·3H<sub>2</sub>O with 25 mL acetonitrile : water (3 : 1) solution in standard volumetric flasks (5 mM). UV–vis and fluorescence measurements were performed by taking appropriate

amount of these stock solutions.

#### 2.2.2. UV–vis absorption measurement

The suitable amount of stock solution of BZ was added to acetonitrile : water (3 : 1) solution (3 mL) in a 3.5 mL quartz cuvette (final concentration = 25 μM). The UV–vis absorption spectra were recorded before and after 15 min incubation time with appropriate amount of Cu (NO<sub>3</sub>)<sub>2</sub>·3H<sub>2</sub>O.

#### 2.2.3. Fluorescence measurement

The suitable amount of stock solution of BZ was added to acetonitrile : water (3 : 1) solution (3 mL) in a 3.5 mL quartz cuvette (final concentration = 25 μM). The fluorescence spectra were recorded before and after 15 min incubation time with appropriate amounts of Cu (NO<sub>3</sub>)<sub>2</sub>·3H<sub>2</sub>O, using the following parameters: excitation wavelength = 332 nm for BZ1, 343 nm for BZ2, 375 nm for BZ3, and 367 nm for BZ4, excitation slit = 10 nm, and emission slit = 10 nm.

### 2.3. Determination of fluorescence quantum yield

Fluorescence quantum yields of the BZ-Cu<sup>2+</sup> complexes were measured in water using quinine sulfate in 0.1 M H<sub>2</sub>SO<sub>4</sub> as a standard (Q<sub>std</sub> = 0.58) and were calculated based on the Eq. (1) [37]:

$$Q = Q_{std} \times \left( \frac{A_{sample}}{A_{std}} \right) \times \left( \frac{I_{std}}{I_{sample}} \right) \times \left( \frac{\eta_{sample}}{\eta_{std}} \right)^2 \quad (1)$$

where Q denotes the fluorescence quantum yields, A is the peak area of emission spectra, I stands for absorption intensities at the excitation wavelength and η is the solvent reflective index.

### 2.4. Binding stoichiometry and binding constant determination

The binding stoichiometry of the complexes between benzothiazole derivatives (BZ2 and BZ3) and Cu<sup>2+</sup> was determined by Job's plot experiments. [38] The samples for Job's plot were prepared by mixing BZ compounds (BZ2 or BZ3) with Cu<sup>2+</sup> at different ratios of BZ over total concentration of BZ and Cu<sup>2+</sup> ([BZ]/([BZ] + [Cu<sup>2+</sup>])) in acetonitrile-water (3:1 v/v) solution, while maintaining the overall concentration of BZ and Cu<sup>2+</sup> ([BZ] + [Cu<sup>2+</sup>]) at 50 μM. The emission intensities of the samples were recorded at 455 nm for BZ2 and 490 nm for BZ3 (excitation wavelength = 343 nm for BZ2 and 375 nm for BZ3). Then, the emission intensities at 455 and 490 nm were plotted against molar fractions of BZ2 and BZ3 ([BZ2]/([BZ2] + [Cu<sup>2+</sup>]) and [BZ3]/([BZ3] + [Cu<sup>2+</sup>])), respectively.

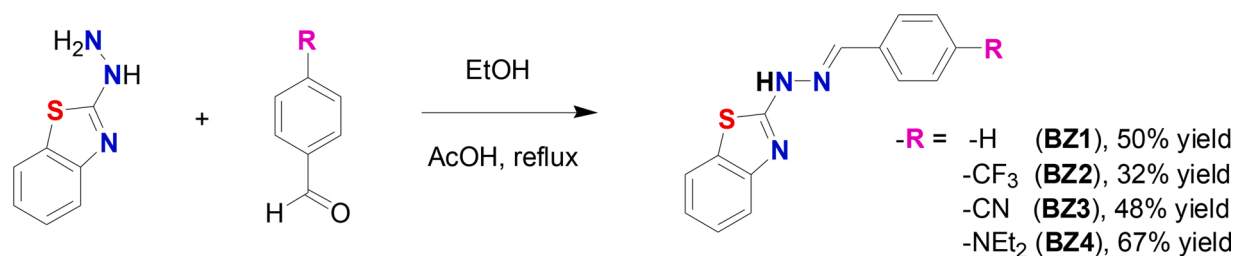
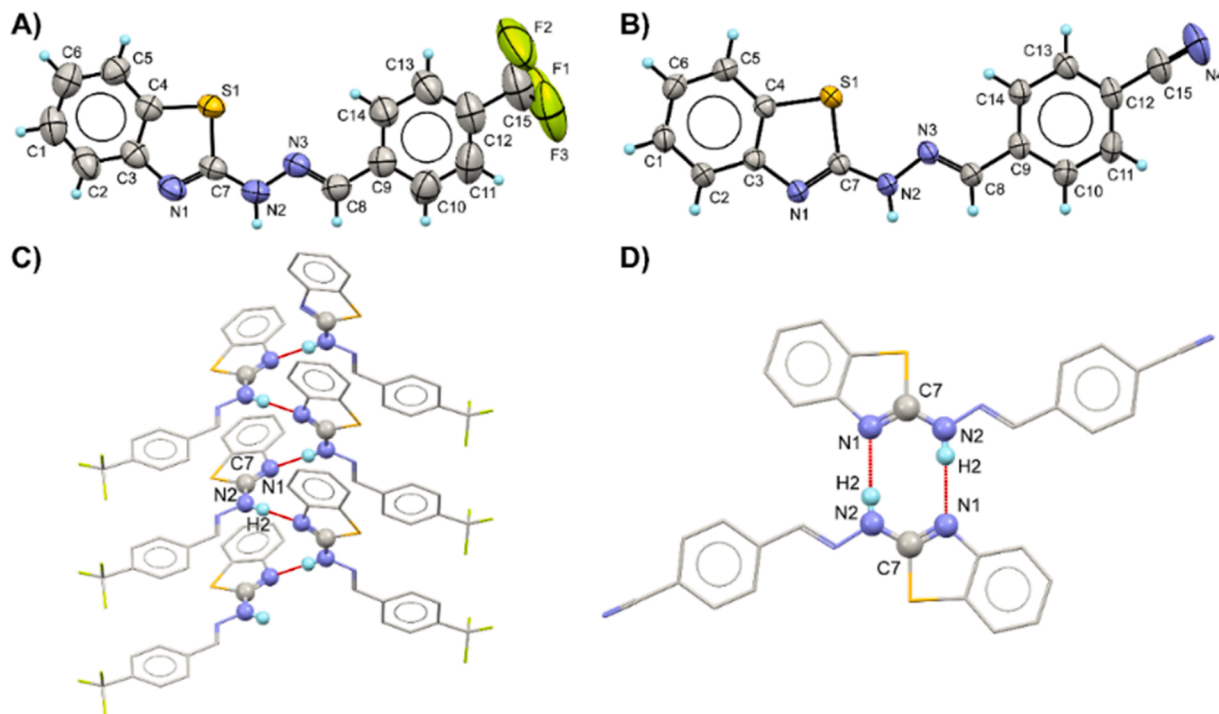
The binding constant values were determined from emission intensities of BZ2 and BZ3 (25 μM) upon the constantly addition of Cu<sup>2+</sup> from 0.1 molar equivalent (2.5 μM) to 1 molar equivalent (25 μM) (0.1 molar equivalent or 2.5 μM increment). The data was fitted to the modified Benesi-Hildebrand Eq. (2) [39]:

$$\frac{1}{F - F_{min}} = \frac{1}{K(F_{max} - F_{min})[Cu^{2+}]} + \frac{1}{F_{max} - F_{min}} \quad (2)$$

where F<sub>min</sub> denotes the emission intensities of benzothiazole-based dyes in the absence of copper ions, F is the emission intensities of the dyes at intermediate copper concentrations, F<sub>max</sub> stands for the emission intensities of the dyes at the complete interaction with copper ions, and K is the binding constant values.

### 2.5. Theoretical calculation

The ground-state geometry optimization of BZ1, BZ2, and BZ3 and their complexes with Cu<sup>2+</sup> (BZ-Cu<sup>2+</sup>) was performed without symmetry constraints. The Becke's three-parameter hybrid exchange functional with the Lee-Yang-Parr gradient-corrected correlation (B3LYP) [40,41]

Scheme 1. The synthesis of **BZ1**, **BZ2**, **BZ3**, and **BZ4**.

**Fig. 2.** The molecular structures of A) **BZ2** (CCD No. 2014836) and B) **BZ3** (CCD No. 2014835) showing the atom-labeling scheme. Displacement ellipsoids are drawn at the 50 % probability level. The non-IUPAC atom labeling is for the convenience of discussion. Views of the crystal packing which illustrate C) the part of C (4) N—H...N hydrogen bonds (red dash lines) in the extended structure of **BZ2** and D) the  $R_2^2(8)$  N—H...N hydrogen bonding loop (red dash lines) between two inversion related molecules of **BZ3**.

and the triple- $\zeta$  valence quality with one set of polarization functions (TZVP) [42] were applied for all atoms except Cu atom. To reduce computational cost, the LANL2DZ effective core potential was applied for the Cu atom to describe the Cu core electrons. The optimized structures and electronic property were then examined in implicit acetonitrile using conductor-like polarized continuum model (C-PCM) framework [43,44]. The frontier molecular orbitals (FMOs) and HOMO-LUMO energy diagrams of **BZs** and **BZ-Cu<sup>2+</sup>** complexes were also calculated at B3LYP/TZVP level of theory. Simulated UV–vis absorption spectra and vertical excitation energy ( $E_{ex}$ ) were carried out using the time-dependent PBE0 function (TD-PBE0) [45] with the same basis set in implicit acetonitrile. This selected method was elucidated in our previous work [46]. All calculations were performed by the Gaussian 16 program package [47].

## 2.6. X-ray absorption spectroscopy (XAS) of the mixtures between $Cu^{2+}$ and **BZ** ligands

To examine the structural information of the binding between the **BZ** ligands and the target  $Cu^{2+}$  ions as well as their complexes, the mixtures between **BZ** ligands and  $Cu(NO_3)_2 \cdot 3H_2O$  in acetonitrile : water 3:1 v/v were characterized by X-ray absorption spectroscopy (XAS) in both X-

ray absorption near edge structure (XANES) and extended X-ray absorption fine structure (EXAFS) analyses. The XAS measurements probed at Cu K-edge were performed at Beamline 1.1 W: Multiple X-ray Techniques, Synchrotron Light Research Institute (SLRI), Thailand. The XAS measurements were conducted in both transmission and fluorescence modes at ambient temperature and pressure by simultaneously measuring the solutions together with the Cu foil as standard reference for an in-line alignment of the energy shift during the synchrotron-operating time. The XAS measurements of  $Cu(NO_3)_2 \cdot 3H_2O$  solution in acetonitrile : water 3:1 v/v was carried out as standard references for comparison with the  $Cu^{2+}$ -**BZ** mixtures. The obtained data were analyzed using ATHENA and ARTEMIS software.

## 3. Results and discussion

### 3.1. Synthesis and crystal structures of benzothiazole derivatives

Novel benzothiazole derivatives featuring electron withdrawing groups (EWG), including, trifluoromethyl (**BZ2**) and cyano (**BZ3**) and electron donating group, such as, diethylamino (**BZ4**) were synthesized by a straightforward and environmental-friendly method as shown in Scheme 1. The known benzothiazole containing phenyl ring (**BZ1**) was

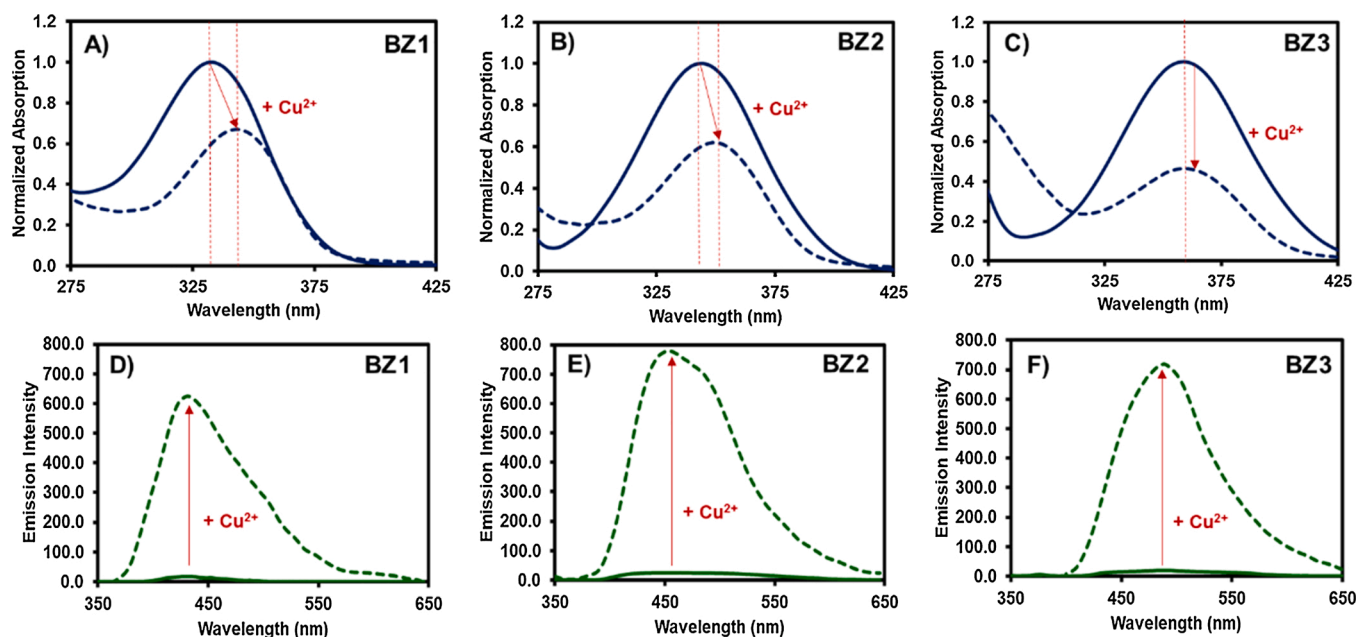


**Fig. 3.** A-C) Absorption spectra of **BZ** derivatives (25  $\mu\text{M}$ ) before and after addition of 1 molar equivalent of  $\text{Cu}^{2+}$  (25  $\mu\text{M}$ ). D-F) Emission spectra of **BZ** derivatives (25  $\mu\text{M}$ ) before and after addition of 1 molar equivalent of  $\text{Cu}^{2+}$  (25  $\mu\text{M}$ ).

also synthesized to use as a reference compound to study the effect of electron tuning substituents toward photophysical properties of the dyes. [48] Their NMR characterizations as well as mass spectrometry results are shown in the supporting information (SI) section.

Furthermore, the structures of **BZ2** and **BZ3** were confirmed by single crystal X-ray diffraction. Crystal data and their corresponding refinement details of the compounds **BZ2** and **BZ3**, are tabulated in **Table S1** and the structural models referring their crystal structures are displayed in **Fig. 2A-B**. The intermolecular interactions within the crystals of **BZ2** and **BZ3** are displayed in **Fig. 2C-D** and listed in **Table S2**. The N—H...N hydrogen bonds were observed in the crystal structures of both compounds. The freely-refined N—H bond distances are 0.89(2) Å and 0.85(2) Å for **BZ2** and **BZ3**, respectively. Although the crystal system and space group of both compound crystals were similar, **BZ2** and **BZ3** possessed the different hydrogen bonding fashions. In the case of **BZ3**, the N—H...N hydrogen bonds linked two molecules related by an inversion center into a dimer creating an  $R_2^2(8)$ -loop motif (**Fig. 2D**). Unlike **BZ3**, the molecules of **BZ2** were joined by the N—H...N hydrogen bonds creating an infinite  $C(4)$  chains propagating along the [010] direction (**Fig. 2C** and **Figure S15**). In addition, the molecular planarity, the  $\pi$ - $\pi$  interactions, and the Hirshfeld surface (HS) analysis of the crystal structures are further explained in the SI section.

### 3.2. Photophysical properties

Firstly, the photophysical properties of **BZ1–3** upon copper ion complexations were investigated to probe the effect of electron withdrawing substituents. As seen in **Fig. 3A-C**, the absorption spectra of all **BZ** derivatives (25  $\mu\text{M}$ ) exhibited the decrease in absorption intensities at 333 nm for **BZ1**, 344 nm for **BZ2** and 360 nm for **BZ3** upon the addition of  $\text{Cu}^{2+}$  (25  $\mu\text{M}$ , 1 molar equivalent) which were similar to those of the pyrene analogue reported in the literature. [36] They also showed the bathochromic shifts of 10 and 5 nm for **BZ1** and **BZ2** and no shift for **BZ3** upon  $\text{Cu}^{2+}$  binding (25  $\mu\text{M}$ , 1 molar equivalent). These results initially confirmed the copper binding for all **BZ** derivatives. It is also important to note that the absorption maxima of free **BZ2** and **BZ3** demonstrated bathochromic shifts of 11 nm and 26 nm compared with that of **BZ1**, respectively (**Figure S20**) due to electron-withdrawing effects from the  $-\text{CF}_3$  and  $-\text{CN}$  groups. These results indicated that the electronic transition energy levels of these **BZ** and **BZ-Cu<sup>2+</sup>** complexes could be tuned by varying electron-withdrawing substituents.

In the emission spectra, **BZ1**, **BZ2**, and **BZ3** displayed increased fluorescent intensities upon the addition of  $\text{Cu}^{2+}$  (**Fig. 3D-F**). Similar to the observation in absorption spectra, the emission maxima of **BZ2-Cu<sup>2+</sup>** and **BZ3-Cu<sup>2+</sup>** showed red shifts of 23 nm and 58 nm from that of **BZ1-Cu<sup>2+</sup>** resulting blue and green fluorescence emission, consecutively

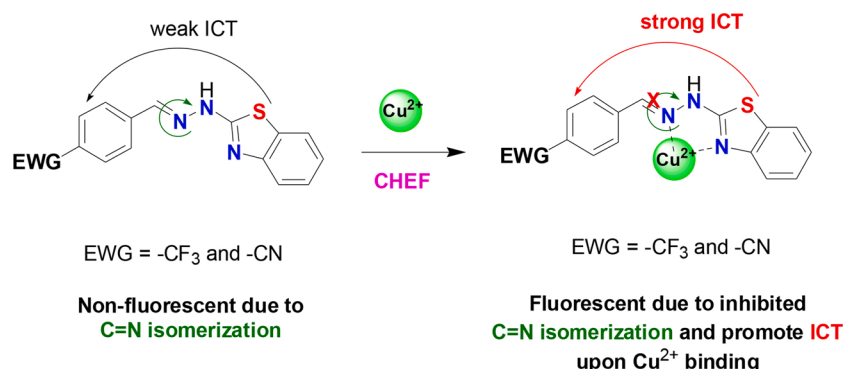


**Fig. 4.** Proposed sensing mechanism for electron-withdrawing substituted benzothiazoles upon copper ion binding.

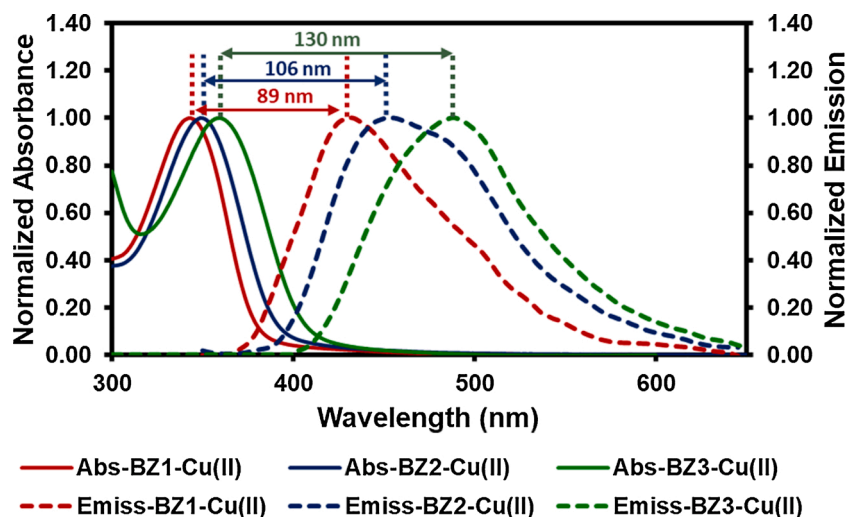


Fig. 5. Absorption, emission spectra, and Stokes shifts of  $\text{BZ-Cu}^{2+}$  complexes.

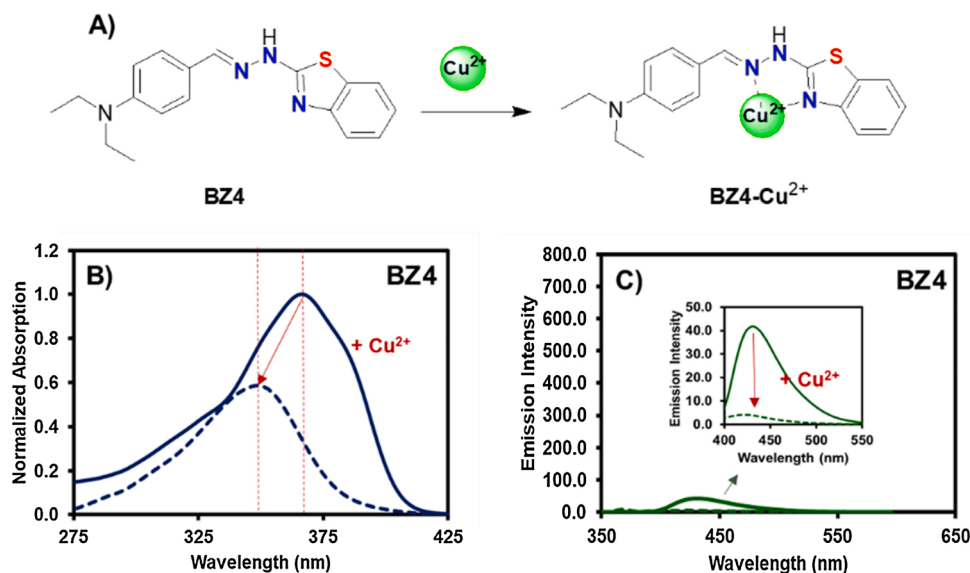


Fig. 6. A) Copper ion complexation reaction of **BZ4**, B) Absorption spectra of **BZ4** (25  $\mu\text{M}$ ) before and after addition of 1 molar equivalent of  $\text{Cu}^{2+}$  (25  $\mu\text{M}$ ), C) Emission spectra of **BZ4** (25  $\mu\text{M}$ ) before and after addition of 1 molar equivalent of  $\text{Cu}^{2+}$  (25  $\mu\text{M}$ ).

(Figure S21). These fluorescence turn-on phenomena could be the results from chelation-induced enhanced fluorescence (CHEF) effect and inhibited  $\text{C} = \text{N}$  isomerization leading to the rigid backbone (Fig. 4). In addition, the intramolecular charge transfer (ICT) process is facilitated over the molecules causing large Stokes' shifts in  $\text{BZ-Cu}^{2+}$  complexes (Fig. 5) suggesting strong ICT effect as seen in other ICT-based fluorescent molecules in the literature. [49–51]

To prove that the ICT mechanism plays a vital role in these fluorescence 'turn-on' processes, the copper ion binding of non-ICT benzothiazole containing electron-donating diethylamino substituent (**BZ4**) was investigated. As displayed in Fig. 6, the **BZ4** underwent fluorescence quenching phenomena upon copper complexation due to paramagnetic effect. The  $\text{BZ4-Cu}^{2+}$  showed the lowest Stokes' shifts in this series (76 nm) indicating weak ICT upon copper complexation. These results confirmed that the fluorescence 'turn-on' processes in **BZ1–3** derivatives upon  $\text{Cu}^{2+}$  binding were caused by the synergistic effect between CHEF and ICT processes. As **BZ2** and **BZ3** are new compounds that possess superior ICT phenomena, they were selected for further studies as copper ion fluorescent sensors.

### 3.3. Sensing properties toward copper ion

The selectivity of **BZ2** and **BZ3** toward various metal cations was investigated by mixing them with 5 equivalents of  $\text{Cu}^{2+}$ ,  $\text{Ca}^{2+}$ ,  $\text{Mg}^{2+}$ ,  $\text{Co}^{2+}$ ,  $\text{Ni}^{2+}$ ,  $\text{Mn}^{2+}$ ,  $\text{Zn}^{2+}$ ,  $\text{Cd}^{2+}$ ,  $\text{Pb}^{2+}$ ,  $\text{Al}^{3+}$ ,  $\text{Fe}^{3+}$ ,  $\text{Cr}^{3+}$ ,  $\text{Ag}^{+}$ , and  $\text{Hg}^{2+}$ , respectively. Their selective fluorescence enhancements by copper ions were observed with a strong blue and green fluorescence emissions (Fig. 7A). The fluorescence spectra of **BZ2** and **BZ3** in the presence of various metal ions were shown in Figure S22 and S23 in the SI section. Subsequently, the effects of interference of the above-mentioned cations on  $\text{Cu}^{2+}$  sensing were also studied. The emission intensities in Fig. 7B suggested that the co-existence of these metal ions does not interfere with  $\text{Cu}^{2+}$  detection in this solvent system. It is also interesting to note that the co-presence of  $\text{Hg}^{2+}$  with  $\text{Cu}^{2+}$  could slightly enhance fluorescence signals in both **BZ2** and **BZ3**.

Next,  $\text{Cu}^{2+}$  titrations with **BZ2** and **BZ3** (25  $\mu\text{M}$ ) were investigated by both absorption and emission techniques. As demonstrated in Fig. 8A–B, when  $\text{Cu}^{2+}$  was constantly added from 0.1 molar equivalent (2.5  $\mu\text{M}$ ) to 1 molar equivalent (25  $\mu\text{M}$ ) of  $\text{Cu}^{2+}$  into the solution of 1 molar equivalent of **BZ** compounds (25  $\mu\text{M}$ ) (0.1 molar equivalent or 2.5  $\mu\text{M}$

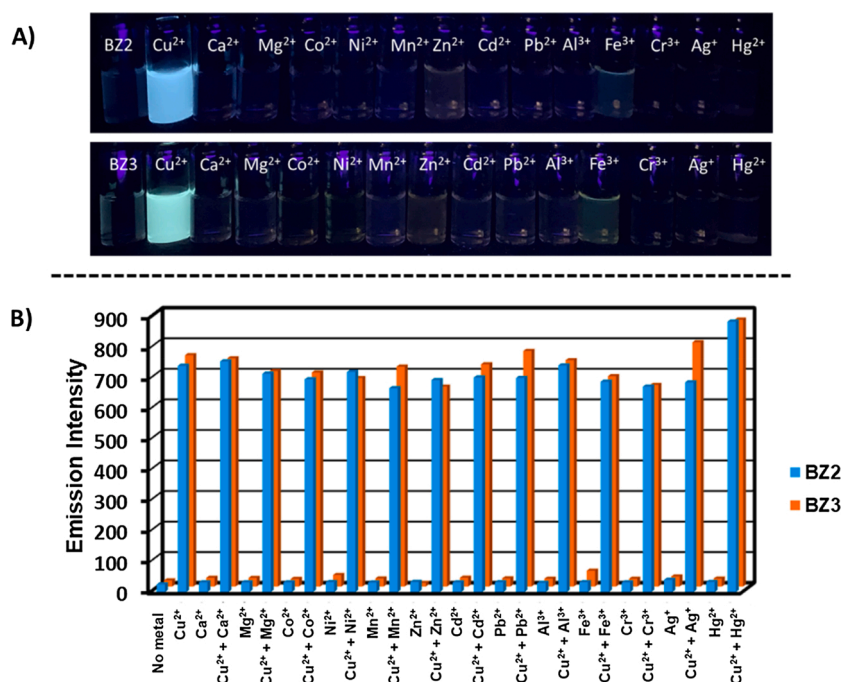


**Fig. 7.** A) Images of **BZ2** and **BZ3** (25  $\mu\text{M}$ ) before and after addition of various metal ions (5 equiv., 125  $\mu\text{M}$ ) in acetonitrile-water ( $v/v = 3:1$ ). B) Bar chart demonstrating fluorescence intensities at 455 nm for **BZ2** and 490 nm for **BZ3** in the presence of different metal ions (selectivity test) and in the presence of  $\text{Cu}^{2+}$  (125  $\mu\text{M}$ ) co-existing with other metal ions (125  $\mu\text{M}$ ) (interfering test).

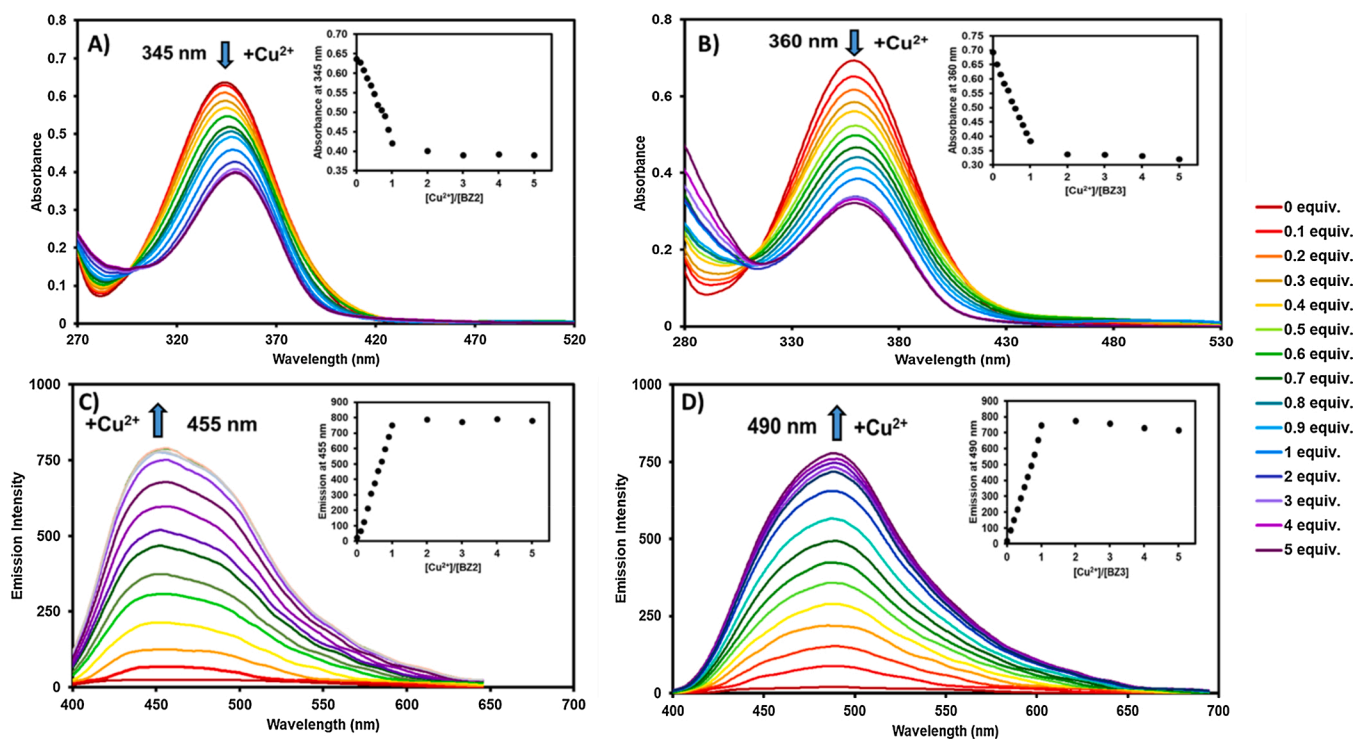


**Fig. 8.** Changes in the absorption spectra of **BZ2** (A), **BZ3** (B) and emission spectra of **BZ2** (C), **BZ3** (D) (excitation wavelength = 343 nm for **BZ2** and 375 nm for **BZ3**) in the presence of various molar equivalents of  $\text{Cu}^{2+}$  in acetonitrile-water (3:1  $v/v$ ) solutions (final concentration of **BZ** compounds = 25  $\mu\text{M}$ ).

increment), the absorption intensities at 344 and 360 nm gradually decreased while the emission intensities at 455 nm and 490 nm gently increased for **BZ2** and **BZ3**, respectively. There were no significant changes in absorption and emission intensities observed after the additions of 2–5 molar equivalents (50–125  $\mu\text{M}$ ) of  $\text{Cu}^{2+}$  to the solution of 1 molar equivalent of **BZ** compounds suggesting 1:1 binding ratios

between these **BZ** ligands and  $\text{Cu}^{2+}$ . The photophysical properties, including, extinction coefficients ( $\epsilon$ ), fluorescence quantum yields ( $\Phi_f$ ), of **BZ2** and **BZ3** before and after addition of  $\text{Cu}^{2+}$  were summarized in [Table 1](#).

The binding stoichiometry of **BZ**- $\text{Cu}^{2+}$  complexes was further confirmed by Job's plot analysis. As display in [Fig. 9A-B](#), the emission

**Table 1**

Photophysical properties of **BZ2** and **BZ3** in in acetonitrile-water (3:1 v/v) solution (1  $\mu\text{M}$ ) before and after addition of  $\text{Cu}^{2+}$ .

Cpd.	Absorption		Emission		Emission with $\text{Cu}^{2+}$ <sup>[a]</sup>	
	$\lambda_{\text{abs}}$	$\epsilon$ ( $\text{M}^{-1} \text{cm}^{-1}$ )	$\lambda_{\text{emiss}}$	$\Phi_f$	$\lambda_{\text{emiss}}$ <sup>[b]</sup>	$\Phi_f$ <sup>[c]</sup> (n = 3)
<b>BZ2</b>	344	$3.4 \times 10^4$	NF <sup>[d]</sup>		455	0.40 ( $\pm 0.025$ )
<b>BZ3</b>	360	$3.1 \times 10^4$	NF		490	0.42 ( $\pm 0.03$ )

<sup>[a]</sup> 1.5  $\mu\text{M}$  of  $\text{Cu}(\text{NO}_3)_2 \cdot 3\text{H}_2\text{O}$  was added.

<sup>[b]</sup> excitation wavelength = 343 nm for **BZ2** and 375 nm for **BZ3**.

<sup>[c]</sup> fluorescence quantum yields estimated by using quinine sulfate in 0.1 M  $\text{H}_2\text{SO}_4$  as a standard ( $\Phi_f = 0.58$ ).

<sup>[d]</sup> NF = non-fluorescence.

intensities at 455 nm and 490 nm were plotted against molar fractions of **BZ2** and **BZ3** ( $[\text{BZ2}]/([\text{BZ2}] + [\text{Cu}^{2+}])$  and  $[\text{BZ3}]/([\text{BZ3}] + [\text{Cu}^{2+}])$ ), while maintaining the total concentrations of **BZ** compound and  $\text{Cu}^{2+}$  ( $[\text{BZ}] + [\text{Cu}^{2+}]$ ) at 50  $\mu\text{M}$ . The maximum emission intensities of both compounds were observed at the mole fractions of 0.5, indicating 1:1 binding ratios of **BZ2**- $\text{Cu}^{2+}$  and **BZ3**- $\text{Cu}^{2+}$  complexes. [38] The detections of molecular ions at  $m/z = 481.0509$   $\{[(\text{BZ2})\text{Cu}(\text{NO}_3)(\text{H}_2\text{O})_2]^+\}$  and 411.0895  $\{[(\text{BZ3-H})\text{Cu}(\text{H}_2\text{O})_4]^+\}$  from electrospray ionization mass spectra (ESI-MS) of the complexes served as the addition proofs of the 1:1 binding stoichiometry of **BZ2** and **BZ3** with  $\text{Cu}^{2+}$  (Figure S13-S14).

The binding constants (K) of **BZ2** and **BZ3** were determined based on Benesi-Hildebrand Eq. (2) by plotting  $1/(F-F_{\text{min}})$  vs.  $1/[\text{Cu}^{2+}]$  as depicted in Fig. 10A-B. The data was linearly fitted, and the K values were calculated as  $2.18 \times 10^4$  and  $3.30 \times 10^4 \text{ M}^{-1}$  for **BZ2** and **BZ3**, respectively. These K values are comparable to that of compound IV and

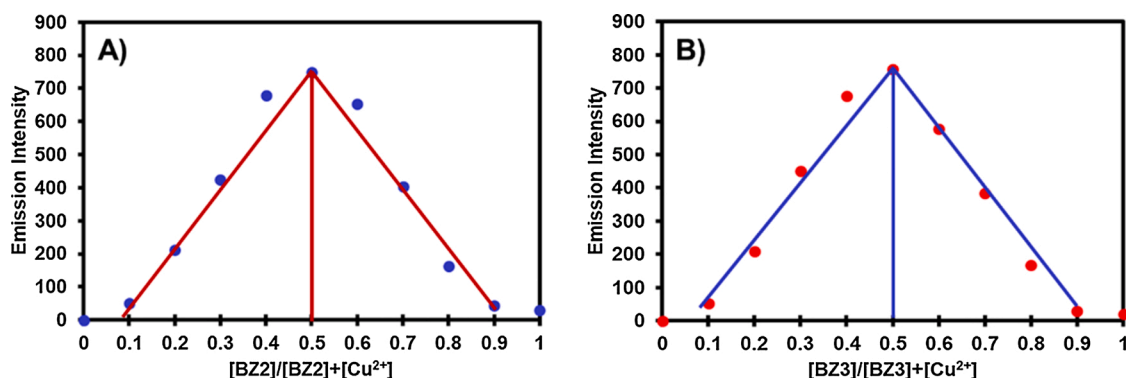


Fig. 9. Job plots for **BZ2** (A) and **BZ3** (B) in acetonitrile-water (3:1 v/v).

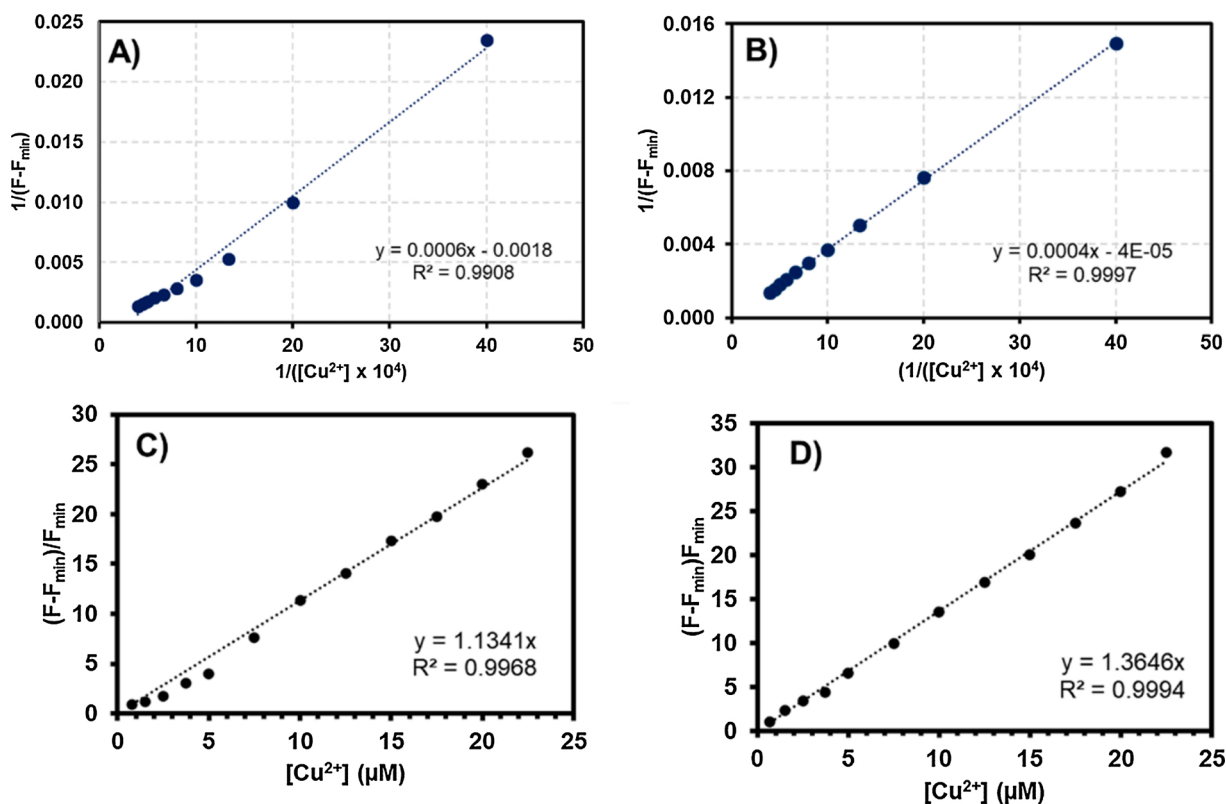


Fig. 10. Binding plots generated from the analysis of fluorescence enhancements of **BZ2** (A) and **BZ3** (B) upon addition of  $\text{Cu}^{2+}$ , and fitted in accordance with Eq. (2), and standard calibration curves demonstrating the fluorescence intensity increment at 455 nm for **BZ2** (C) and 490 nm for **BZ3** (D) as a function of copper concentrations.  $F_{\text{min}}$  = Emission intensities of the benzothiazole-based dyes in the absence of copper ions.

**Table 2**

Comparison of **BZ2** and **BZ3** with other reported benzothiazole-based sensors for copper ion detection.

Sensor	Solvent system	LOD (ppb)	Binding Constant (K) (binding mode: Cu <sup>2+</sup> : ligand)	Sensing mechanism	Reference
I	Acetonitrile-water (3:1 v/v)	2.73 μM	$5.00 \times 10^8 \text{ M}^{-2}$ (1:2)	Turn-on	[36]
II	Acetonitrile	0.014 μM	N.R.	Turn-off	[32]
III	Acetonitrile-water (4:1 v/v)	1.05 μM	$2.92 \times 10^{10} \text{ M}^{-2}$ (2:1)	Turn-off	[34]
IV	DMSO-water (2:98v/v)	2.4 nM	$7.78 \times 10^4 \text{ M}^{-1}$ (1:1)	Turn-off	[31]
V	Acetonitrile-water (1:1 v/v)	0.36 μM	$5.70 \times 10^6 \text{ M}^{-1}$ (1:1)	Turn-off	[33]
VI	Acetonitrile-water (9:1 v/v)	N.R.	$5.06 \times 10^6 \text{ M}^{-1}$ (1:1)	Turn-off	[35]
<b>BZ2</b>	Acetonitrile-water (3:1 v/v)	0.77 μM	$2.18 \times 10^4 \text{ M}^{-1}$ (1:1)	Turn-on	This work
<b>BZ3</b>	Acetonitrile-water (3:1 v/v)	0.64 μM	$3.30 \times 10^4 \text{ M}^{-1}$ (1:1)	Turn-on	This work

N.R. = Not Report.

slightly lower than those of compound **V** and **VI** in the literature (Table 2). Next, the limits of detection (LOD) of these chemosensors were determined from the plots of emission intensities ( $F_{\text{min}}/F_{\text{min}}$ )/ $F_{\text{min}}$  and Cu<sup>2+</sup> concentrations as demonstrated in Fig. 10C-D by employing  $3\sigma/m$  formula, where  $\sigma$  is the standard deviation of fluorescence signals of sensors in the absence of Cu<sup>2+</sup> and  $m$  is the slopes of the plots. The LODs of **BZ2** and **BZ3** were calculated as 0.77 and 0.64 μM, respectively. Compared with the LODs of other benzothiazole-based sensors in the literature, the LODs of **BZ2** and **BZ3** were lower than those of pyrene-linked benzothiazole (sensor I) and calix [4]arene appended benzothiazole (Sensor III) (Table 2).

The effect of pH toward Cu<sup>2+</sup> binding of **BZ2** and **BZ3** was investigated in acetonitrile-standard buffer solution (3:1 v/v) in the pH range of 1–12. As displayed in Fig. 11, these **BZ** compounds worked well in neutral pH condition (pH = 7) as they demonstrated distinct fluorescent intensity change upon Cu<sup>2+</sup> binding. This result suggested the suitable pH value for the Cu<sup>2+</sup> ion detection in real water samples using these probes. There were no fluorescence signals observed at the acidic pHs (pH 1–6) with and without the presence of copper ion which could be the results from the protonations at the imine and the nitrogen atom in the five-membered ring as seen in the literature. [28] These protonations could block both electron conjugation and metal binding of **BZ**

compounds in acetonitrile/water media.

### 3.4. Theoretical calculations

To further understand the electronic and photophysical properties of **BZ** and **BZ-Cu<sup>2+</sup>** complexes, the DFT calculations were performed using B3LYP/TZVP level of theory in the implicit solvent of acetonitrile and the LANL2DZ basis set for Cu<sup>2+</sup>. The optimized structures as well as the calculated highest occupied molecular orbital (HOMO), lowest unoccupied molecular orbital (LUMO) energy levels, and the HOMO-LUMO energy gap of the **BZ1-3** and **BZ1-3-Cu<sup>2+</sup>** are presented in Fig. 12. Comparing among free **BZ** ligands, the HOMO-LUMO energy gaps decreased from **BZ1** to **BZ3** ( $\Delta E = 3.96, 3.76,$  and  $3.54 \text{ eV}$ , for **BZ1**, **BZ2**, and **BZ3**, respectively), as the electron withdrawing groups (-CF<sub>3</sub>, and -CN) could stabilize the LUMO levels effectively. The LUMO isosurface diagrams of **BZ2** and **BZ3** demonstrated larger electron distributions on CF<sub>3</sub>- and CN-substituted phenylene indicating weak ICT in these molecules. When Cu<sup>2+</sup> interacted with nitrogen donor atoms in the ICT-based compounds, such as **BZ2** and **BZ3**, the ground states of **BZ2-Cu<sup>2+</sup>** and **BZ3-Cu<sup>2+</sup>** are more stabilized than the excited state leading to larger energy gaps of **BZ2-Cu<sup>2+</sup>** and **BZ3-Cu<sup>2+</sup>** comparing to those of **BZ2** and **BZ3** [49]. These computational results are consistent with the experimental outcomes that the **BZ1** displayed the highest red shift upon Cu<sup>2+</sup> binding (Fig. 3A-C). The changes of HOMO and LUMO diagrams in **BZ2-Cu<sup>2+</sup>** and **BZ3-Cu<sup>2+</sup>** showed distinct electron density moves distributing from benzothiazole units in the HOMOs to CF<sub>3</sub>- and CN-connected phenylene groups in the LUMOs, respectively, suggesting a strong ICT effect in these complexes.

Next, the UV-vis spectra of **BZ1**, **BZ2**, **BZ3**, **BZ1-Cu<sup>2+</sup>**, **BZ2-Cu<sup>2+</sup>**, and **BZ3-Cu<sup>2+</sup>** were calculated using time-dependent density functional theory (TD-DFT) calculations in an acetonitrile medium. The simulated absorption peaks obtained from TD-PBE0/TZVP level of theory (Figure S24-S29) agreed well with the experimentally obtained peaks as seen in Table 3. The simulated results by this TD-PBE0/TZVP method indicated that the electronic transitions of **BZ1-3** are predominantly contributed from HOMO-LUMO transitions with up to 99 % contributions while the electronic transitions of **BZ1-Cu<sup>2+</sup>**, **BZ2-Cu<sup>2+</sup>**, and **BZ3-Cu<sup>2+</sup>** complexes are mainly contributed from the HOMO-LUMO and the HOMO-LUMO+1 transitions.

### 3.5. Revealing structural binding of **BZ** ligands with targeted Cu<sup>2+</sup> by XAS

XAS measurements probed at the Cu K-edge were carried out in both XANES and EXAFS regions to identify the structural information of the binding between the **BZ** ligands and the targeted Cu<sup>2+</sup> ions. XANES spectra (Fig. 13A) reveals the significantly different fingerprint patterns of the equimolar **BZ1-Cu<sup>2+</sup>**, **BZ2-Cu<sup>2+</sup>**, and **BZ3-Cu<sup>2+</sup>** mixtures in acetonitrile : water of 3:1 v/v from the one of Cu(NO<sub>3</sub>)<sub>2</sub>·3H<sub>2</sub>O solution in the same solvent system. Moreover, EXAFS data of the **BZ-Cu<sup>2+</sup>**

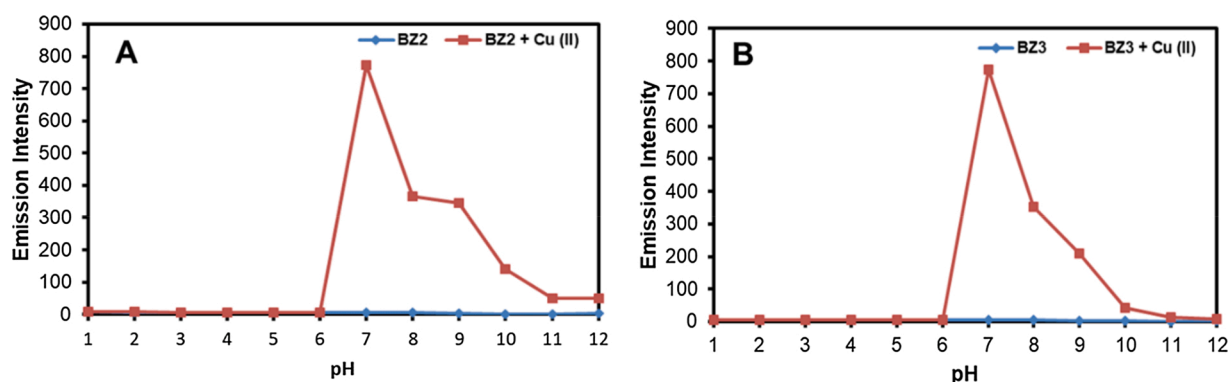


Fig. 11. Fluorescence intensity variation at maximum emission of 455 nm for **BZ2** (A) and 490 nm for **BZ3** (B) at media alternation of pH from 1 to 12.

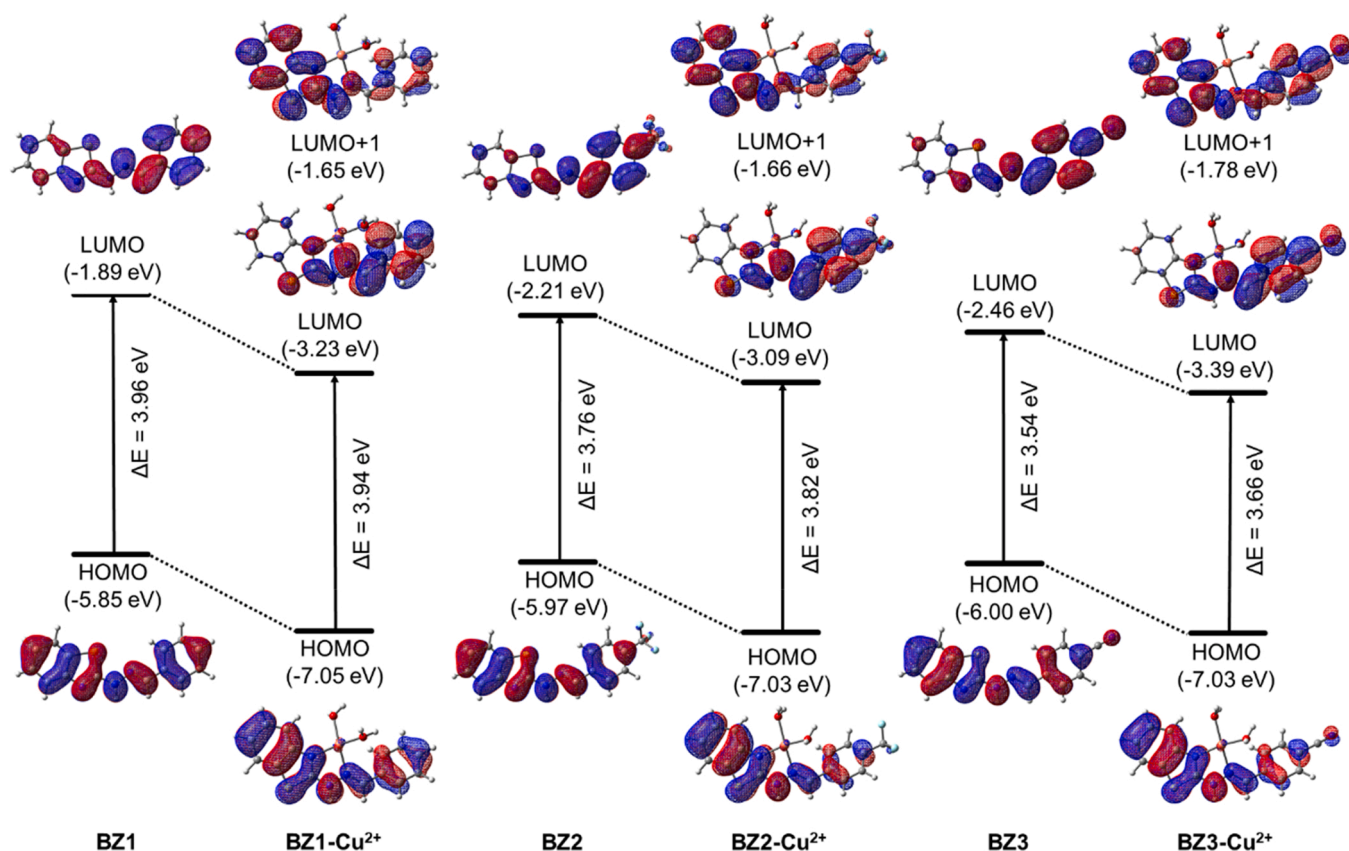


Fig. 12. Frontier molecular orbitals (HOMO and LUMO) of **BZ1**, **BZ1-Cu<sup>2+</sup>**, **BZ2**, **BZ2-Cu<sup>2+</sup>**, **BZ3**, and **BZ3-Cu<sup>2+</sup>** and energy gaps ( $\Delta E$  in eV) computed by B3LYP/TZVP level of theory. The HOMO and LUMO orbitals are plotted with isovalue of 0.02.

Table 3

Comparison of calculated UV-vis absorption wavelength ( $\lambda_{\text{cal}}$ ), experimental UV-vis absorption wavelength ( $\lambda_{\text{exp}}$ ), excitation energies ( $E_{\text{ex}}$ ), oscillator strengths ( $f$ ), and molecular orbital contributions (MOs) of **BZ1**, **BZ2**, **BZ3**, **BZ1-Cu<sup>2+</sup>**, **BZ2-Cu<sup>2+</sup>**, and **BZ3-Cu<sup>2+</sup>**. The calculation obtained from TD-PBE0/TZVP level of theory in implicit acetonitrile.

Compound	Electronic and photophysical properties				
	$\lambda_{\text{cal}}$ (nm)	$\lambda_{\text{exp}}$ (nm)	$E_{\text{ex}}$ (eV)	$f$	MOs (% Contributions)
<b>BZ1</b>	339	333	3.65	1.0466	HOMO→LUMO (99%)
<b>BZ2</b>	355	344	3.49	1.0040	HOMO→LUMO (99%)
<b>BZ3</b>	376	360	3.30	1.0565	HOMO→LUMO (99%)
<b>BZ1-Cu<sup>2+</sup></b>	350	343	3.54	0.5752	HOMO→LUMO (47 %), HOMO→LUMO+1 (49 %)
<b>BZ2-Cu<sup>2+</sup></b>	357	349	3.48	0.5222	HOMO→LUMO (49 %), HOMO→LUMO+1 (46 %)
<b>BZ3-Cu<sup>2+</sup></b>	372	360	3.33	0.4397	HOMO→LUMO (37 %), HOMO→LUMO+1 (41 %)

mixtures shown in k-space (Fig. 13B) and R-space (Fig. 13C) exhibit the deviation of oscillation pattern and the radial distance distribution from the aqua-based Cu<sup>2+</sup> complex. This observation clearly confirms that the targeted Cu<sup>2+</sup> are bound to the **BZ** ligands and form the **BZ-Cu<sup>2+</sup>** complexes. To get insight into the structural information of the **BZ1-Cu<sup>2+</sup>**, **BZ2-Cu<sup>2+</sup>**, and **BZ3-Cu<sup>2+</sup>** complexes, the detailed analysis of XANES and EXAFS fitting using the structural model obtained from DFT calculation are further examined (Figure S30 and Table S3). The pronounced pre-edge peak at about 8980 eV reflects the quadrupole allowed 1s-3d transitions, which reveals a non-centrosymmetric environment of Cu<sup>2+</sup> due to the 3d-4p orbital mixing. [52,53] Note that, the pre-edge at 8980 eV is not observed in the case of aqua-based Cu<sup>2+</sup>

complex consisting of 6 H<sub>2</sub>O ligands coordinated to Cu<sup>2+</sup> in octahedral geometry. According to the structural optimization based on DFT calculation, the 4-coordinated non-centrosymmetric **BZ-Cu<sup>2+</sup>** complexes are suggested. The EXAFS fittings using these structural models indicate the well-matched of the 4-coordinated non-centrosymmetric **BZ-Cu<sup>2+</sup>** structural models with the experimental data (Figure S30 and Table S3). In all, XANES and EXAFS data of the **BZ-Cu<sup>2+</sup>** mixtures exhibit the binding between Cu<sup>2+</sup> and the **BZ** ligands with a 1:1 ratio in a 4-coordinated non-centrosymmetric fashion.

#### 4. Conclusions

In summary, we have synthesized new Schiff base ligands containing the benzothiazolyl hydrazone acting as a metal ion binding site and an electron donor moiety and the electron withdrawing trifluoromethyl and cyano substituted phenylene as an electron acceptor. These derivatives exhibited selective fluorescence ‘turn-on’ responses toward copper ion binding due to the synergistic phenomena between the chelation-enhanced fluorescence (CHEF) and the intramolecular charge transfer (ICT) processes. The job plots, Benesi-Hildebrand analysis and the XAS analysis confirmed 1:1 binding mode between copper ion and the ligands with the binding constants of  $2.18 \times 10^4 \text{ M}^{-1}$  and  $3.30 \times 10^4 \text{ M}^{-1}$  for **BZ2** and **BZ3**, respectively. The low limits of detections ( $0.77 \mu\text{M}$  for **BZ2** and  $0.64 \mu\text{M}$  for **BZ3**), their Cu<sup>2+</sup> binding capability at the physiological pH and their interference studies suggested the potential of these compounds for Cu<sup>2+</sup> analysis in real water samples, such as, tap water, drinking water, and natural water. The density functional theory (DFT) and the time-dependent density functional theory (TD-DFT) calculations indicated strong accepting ability of trifluoromethyl and cyano group leading to lower HOMO-LUMO energy gaps and bathochromic shifts in **BZ2** and **BZ3** compared with the non-substituted phenylene derivative (**BZ1**). The electron density movements from the HOMOs to

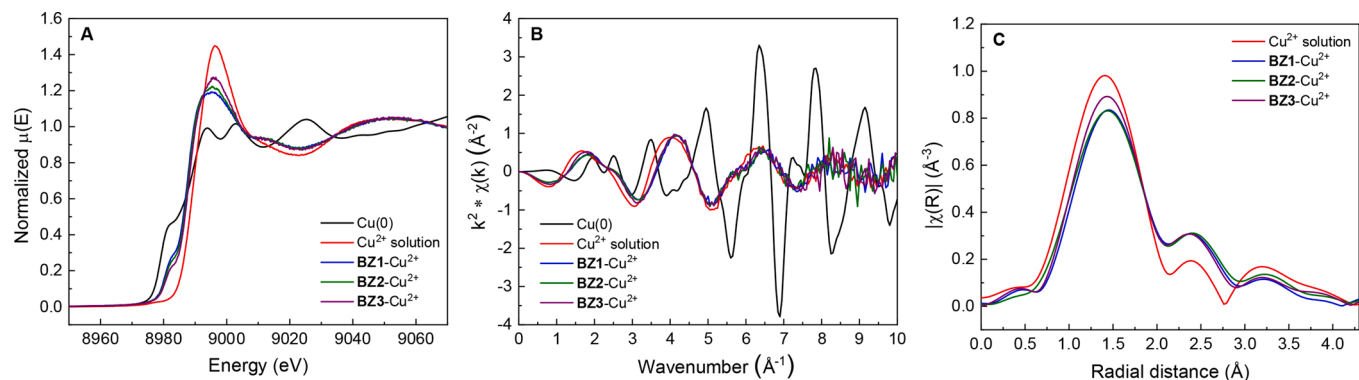


**Fig. 13.** XANES spectra probed at Cu K-edge of the mixtures of BZ1-Cu<sup>2+</sup>, BZ2-Cu<sup>2+</sup>, and BZ3-Cu<sup>2+</sup> in acetonitrile : water 3:1 v/v comparing with Cu(NO<sub>3</sub>)<sub>2</sub>·3H<sub>2</sub>O solution and the standard Cu foil (A) and the corresponding EXAFS data plotted in k-space (B) and the corresponding Fourier-transformed R-space from the k range of 3 – 7.5 Å<sup>-1</sup> (C).

the LUMOs in BZ2-Cu<sup>2+</sup> and BZ3-Cu<sup>2+</sup> as well as their large Stokes shifts confirmed the strong ICT process after Cu<sup>2+</sup> binding which play vital role in fluorescence ‘turn-on’ mechanism.

#### CRediT authorship contribution statement

**Jukkrit Nootem:** Methodology, Investigation, Validation, Writing - original draft. **Rathawat Daengngern:** Investigation, Validation, Writing - review & editing. **Chanchai Sattayanon:** Formal analysis, Writing - review & editing. **Worawat Wattanathana:** Formal analysis, Writing - review & editing. **Suttipong Wannapaiboon:** Formal analysis, Writing - review & editing. **Paitoon Rashatasakhon:** Resources, Supervision. **Kantapat Chansaenpak:** Conceptualization, Methodology, Resources, Supervision, Project administration, Funding acquisition, Writing - review & editing.

#### Declaration of Competing Interest

The authors declare that they have no known competing financial interests or personal relationships that could have appeared to influence the work reported in this paper.

#### Acknowledgments

This work has been financially supported by the Research Network of NANOTEC (RNN) program of the National Nanotechnology Center (NANOTEC), NSTDA, Ministry of Higher Education, Science, Research, and Innovation, Thailand (Grant No. P1851658) and Thailand Development and Promotion of Science and Technology Talents Project (DPST Research Grant 007/2559). Synchrotron Light Research Institute, Thailand is also acknowledged for the provision of XAS beamtime at the Beamline 1.1 W (Multiple X-ray Techniques, MXT).

#### Appendix A. Supplementary data

Supplementary material related to this article can be found, in the online version, at doi:<https://doi.org/10.1016/j.jphotochem.2021.113318>.

#### References

- [1] J.A. Cowan, *Inorganic Biochemistry: An Introduction*, Wiley-VCH, New York, 1997.
- [2] V. Desai, S.G. Kaler, Role of copper in human neurological disorders, *Am. J. Clin. Nutr.* 88 (3) (2008), 855S-8S.
- [3] K. Ghosh, D. Kar, Anthraquinone coupled benzothiazole-based receptor for selective sensing of Cu<sup>2+</sup>, *J. Incl. Phenom. Macrocycl. Chem.* 77 (1) (2013) 67–74.
- [4] Y. Zheng, K.M. Gattás-Asfura, V. Konka, R.M. Leblanc, A dansylated peptide for the selective detection of copper ions, *Chem. Commun.* (20) (2002) 2350–2351.

- [5] M. Saleem, M. Rafiq, M. Hanif, M.A. Shaheen, S.-Y. Seo, A brief review on fluorescent copper sensor based on conjugated organic dyes, *J. Fluoresc.* 28 (1) (2018) 97–165.
- [6] S. Chowdhury, B. Roop, A. Dutta, U. Mandal, Review on recent advances in metal ions sensing using different fluorescent probes, *J. Fluoresc.* 28 (4) (2018) 999–1021.
- [7] K.P. Carter, A.M. Young, A.E. Palmer, Fluorescent sensors for measuring metal ions in living systems, *Chem. Rev.* 114 (8) (2014) 4564–4601.
- [8] E.V. Antina, N.A. Bumagina, A.I. V'Yugin, A.V. Solomonov, Fluorescent indicators of metal ions based on dipyrromethene platform, *Dye. Pigment.* 136 (2017) 368–381.
- [9] A. Torrado, G.K. Walkup, B. Imperiali, Exploiting polypeptide motifs for the design of selective Cu(II) ion chemosensors, *J. Am. Chem. Soc.* 120 (3) (1998) 609–610.
- [10] G. Klein, D. Kaufmann, S. Schürch, J.-L. Reymond, A fluorescent metal sensor based on macrocyclic chelation, *Chem. Commun.* (6) (2001) 561–562.
- [11] M. Boiocchi, L. Fabbrizzi, M. Licchelli, D. Sacchi, M. Vázquez, C. Zampa, A two-channel molecular dosimeter for the optical detection of copper(II), *Chem. Commun.* (15) (2003) 1812–1813.
- [12] Y. Zheng, J. Orbulescu, X. Ji, F.M. Andreopoulos, S.M. Pham, R.M. Leblanc, Development of fluorescent film sensors for the detection of divalent copper, *J. Am. Chem. Soc.* 125 (9) (2003) 2680–2686.
- [13] B.C. Roy, B. Chandra, D. Hromas, S. Mallik, Synthesis of new, pyrene-containing, metal-chelating lipids and sensing of cupric ions, *Org. Lett.* 5 (1) (2003) 11–14.
- [14] S.H. Kim, J.S. Kim, S.M. Park, S.-K. Chang, Hg<sup>2+</sup>-Selective OFF-ON and Cu<sup>2+</sup>-Selective ON-OFF type fluoroionophore based upon cyclam, *Org. Lett.* 8 (3) (2006) 371–374.
- [15] J. Chan, S.C. Dodani, C.J. Chang, Reaction-based small-molecule fluorescent probes for chemoselective bioimaging, *Nat. Chem.* 4 (12) (2012) 973–984.
- [16] K. Chansaenpak, A. Kamkaew, O. Weeranantapan, K. Suttisintong, G. Tumcharern, Coumarin probe for selective detection of fluoride ions in aqueous solution and its bioimaging in live cells, *Sensors* 18 (7) (2018).
- [17] Y. Dong, R. Fan, W. Chen, P. Wang, Y. Yang, A simple quinolone Schiff-base containing CHEF based fluorescence ‘turn-on’ chemosensor for distinguishing Zn<sup>2+</sup> and Hg<sup>2+</sup> with high sensitivity, selectivity and reversibility, *J. Chem. Soc. Dalton Trans.* 46 (20) (2017) 6769–6775.
- [18] S.R. Bhatta, B. Mondal, G. Vijaykumar, A. Thakur, ICT-isomerization-Induced turn-on fluorescence probe with a large emission shift for mercury ion: application in combinational molecular logic, *Inorg. Chem.* 56 (19) (2017) 11577–11590.
- [19] V. Kumar, A. Kumar, U. Diwan, Ramesh Shweta, S.K. Srivastava, et al., Salicylideneimines as efficient dual channel emissive probes for Al<sup>3+</sup>: harnessing ESIPt and ICT processes, *Sens. Actuators B Chem.* 207 (2015) 650–657.
- [20] P. Sontisiri, P. Yingyuad, P. Thongyoo, A highly selective ‘Turn On’ fluorescent probe based on FRET mechanism for hydrogen sulfide detection in living cells, *J. Photochem. Photobiol. A: Chem.* 391 (2020), 112401.
- [21] S.R. Goswami, K. Aich, S. Das, C. Das Mukhopadhyay, D. Sarkar, T.K. Mondal, A new visible-light-excitable ICT-CHEF-mediated fluorescence ‘turn-on’ probe for the selective detection of Cd<sup>2+</sup> in a mixed aqueous system with live-cell imaging, *J. Chem. Soc. Dalton Trans.* 44 (12) (2015) 5763–5770.
- [22] C. Chang, F. Wang, J. Qiang, Z. Zhang, Y. Chen, W. Zhang, et al., Benzothiazole-based fluorescent sensor for hypochlorite detection and its application for biological imaging, *Sens. Actuators B Chem.* 243 (2017) 22–28.
- [23] X. Gong, X. Ding, N. Jiang, T. Zhong, G. Wang, Benzothiazole-based fluorescence chemosensors for rapid recognition and ‘turn-off’ fluorescence detection of Fe<sup>3+</sup> ions in aqueous solution and in living cells, *Microchem. J.* 152 (2020), 104351.
- [24] D. Musib, M.K. Raza, S.S. Devi, M. Roy, A reversible, benzothiazole-based ‘Turn-on’ fluorescence sensor for selective detection of Zn<sup>2+</sup> ions in vitro, *J. Chem. Sci.* 132 (1) (2020) 43.
- [25] Y. Chen, T. Wei, Z. Zhang, T. Chen, J. Li, J. Qiang, et al., A benzothiazole-based fluorescent probe for ratiometric detection of Al<sup>3+</sup> in aqueous medium and living cells, *Ind. Eng. Chem. Res.* 56 (43) (2017) 12267–12275.
- [26] C. Chang, F. Wang, T. Wei, X. Chen, Benzothiazole-based fluorescent sensor for ratiometric detection of Zn(II) ions and secondary sensing PPI and its applications

- for biological imaging and PPase catalysis assays, *Ind. Eng. Chem. Res.* 56 (31) (2017) 8797–8805.
- [27] L. Wang, X. Chen, Q. Xia, R. Liu, J. Qu, Deep-red AIE-Active fluorophore for hypochlorite detection and bioimaging in live cells, *Ind. Eng. Chem. Res.* 57 (23) (2018) 7735–7741.
- [28] V. Kachwal, I.S. Vamsi Krishna, L. Fageria, J. Chaudhary, R. Kinkar Roy, R. Chowdhury, et al., Exploring the hidden potential of a benzothiazole-based Schiff-base exhibiting AIE and ESIPT and its activity in pH sensing, intracellular imaging and ultrasensitive & selective detection of aluminium (Al<sup>3+</sup>), *Analyst* 143 (15) (2018) 3741–3748.
- [29] K. Chauhan, P. Singh, B. Kumari, R.K. Singhal, Synthesis of new benzothiazole Schiff base as selective and sensitive colorimetric sensor for arsenic on-site detection at ppb level, *Anal. Methods* 9 (11) (2017) 1779–1785.
- [30] C. Sravani, A. Sivaramakrishna, Benzothiazole-based sensors for protons and chromium(III) ions, *ChemistrySelect*. 2 (20) (2017) 5688–5694.
- [31] B. Gu, L. Huang, W. Su, X. Duan, H. Li, S. Yao, A benzothiazole-based fluorescent probe for distinguishing and bioimaging of Hg<sup>2+</sup> and Cu<sup>2+</sup>, *Anal. Chim. Acta* 954 (2017) 97–104.
- [32] K. Wang, W. Feng, Y. Wang, D. Cao, R. Guan, X. Yu, et al., A coumarin derivative with benzothiazole Schiff's base structure as chemosensor for cyanide and copper ions, *Inorg. Chem. Commun.* 71 (2016) 102–104.
- [33] Y.B. Wagh, A. Kuwar, S.K. Sahoo, J. Gallucci, D.S. Dalal, Highly selective fluorimetric sensor for Cu<sup>2+</sup> and Hg<sup>2+</sup> using a benzothiazole-based receptor in semi-aqueous media and molecular docking studies, *RSC Adv.* 5 (56) (2015) 45528–45534.
- [34] S. Erdemir, B. Tabakci, M. Tabakci, A highly selective fluorescent sensor based on calix[4]arene appended benzothiazole units for Cu<sup>2+</sup>, S<sup>2-</sup> and HSO<sub>4</sub><sup>-</sup> ions in aqueous solution, *Sens. Actuators B Chem.* 228 (2016) 109–116.
- [35] N. Kaur, J. Singh, G. Dhaka, R. Rani, V. Luxami, Benzothiazole-based chemosensor for CN<sup>-</sup> and Cu<sup>2+</sup>: multi-logic operations within a single molecule, *Supramol. Chem.* 27 (7-8) (2015) 453–459.
- [36] H.-F. Wang, S.-P. Wu, A pyrene-based highly selective turn-on fluorescent sensor for copper(II) ions and its application in living cell imaging, *Sens. Actuators B Chem.* 181 (2013) 743–748.
- [37] K. Chansaenpak, H. Wang, M. Wang, B. Giglio, X. Ma, H. Yuan, et al., Synthesis and evaluation of [18F]-Ammonium BODIPY dyes as potential positron emission tomography agents for myocardial perfusion imaging, *Chem. Eur. J.* 22 (34) (2016) 12122–12129.
- [38] Y. Li, X. Han, Y. Song, An azo-phenol derivative probe: colorimetric and “turn-on” fluorescent detection of copper(II) ions and pH value in aqueous solution, *RSC Adv.* 7 (33) (2017) 20537–20541.
- [39] Li C-r, Qin J-c, Wang G-q, Wang B-d, Z.-y. Yang, A novel pyrazine derivative as a “turn on” fluorescent sensor for the highly selective and sensitive detection of Al<sup>3+</sup>, *Anal. Methods* 7 (8) (2015) 3500–3505.
- [40] A.D. Becke, Density-functional thermochemistry. III. The role of exact exchange, *J. Chem. Phys.* 98 (7) (1993) 5648–5652.
- [41] P.J. Stephens, F.J. Devlin, C.F. Chabalowski, M.J. Frisch, Ab initio calculation of vibrational absorption and circular dichroism spectra using density functional force fields, *J. Phys. Chem.* 98 (45) (1994) 11623–11627.
- [42] A. Schäfer, H. Horn, R. Ahlrichs, Fully optimized contracted Gaussian basis sets for atoms Li to Kr, *J. Chem. Phys.* 97 (4) (1992) 2571–2577.
- [43] M. Cossi, V. Barone, Time-dependent density functional theory for molecules in liquid solutions, *J. Chem. Phys.* 115 (10) (2001) 4708–4717.
- [44] P. Ordon, A. Tachibana, Investigation of the role of the C-PCM solvent effect in reactivity indices, *J. Chem. Sci. Bangalore (Bangalore)* 117 (5) (2005) 583–589.
- [45] C. Adamo, V. Barone, Toward reliable density functional methods without adjustable parameters: the PBE0 model, *J. Chem. Phys.* 110 (13) (1999) 6158–6170.
- [46] J. Nootem, C. Sattayanon, S. Namuangruk, P. Rashatasakorn, W. Wattanathana, G. Tumcharern, et al., Solvatochromic triazaborolopyridinium probes toward ultra-sensitive trace water detection in organic solvents, *Dye. Pigment.* 181 (2020), 108554.
- [47] M.J. Frisch, G.W. Trucks, H.B. Schlegel, G.E. Scuseria, M.A. Robb, J.R. Cheeseman, et al., *Gaussian 16 Rev. B.01* (2016). Wallingford CT.
- [48] A.C. Pinheiro, M.V.N. de Souza, M.C.S. Lourenço, C.F. da Costa, T.C. Baddeley, J. N. Low, et al., Synthesis, potent anti-TB activity against M. Tuberculosis ATCC 27294, crystal structures and complex formation of selected 2-arylidenehydrazinylbenzothiazole derivatives, *J. Mol. Struct.* 1178 (2019) 655–668.
- [49] S. Sahana, G. Mishra, S. Sivakumar, P.K. Bharadwaj, 2-(2'-Hydroxyphenyl)-benzothiazole (HBT)-terpyridine conjugate: a highly specific ICT based fluorescent probe for Zn<sup>2+</sup> ions and its application in confocal cell imaging, *J. Photochem. Photobiol. A: Chem.* 351 (2018) 231–239.
- [50] M. Zhu, Y. Xu, L. Sang, Z. Zhao, L. Wang, X. Wu, et al., An ICT-based fluorescent probe with a large Stokes shift for measuring hydrazine in biological and water samples, *Environ. Pollut.* 256 (2020), 113427.
- [51] X. Ren, F. Zhang, H. Luo, L. Liao, X. Song, W. Chen, Red-emitting boron difluoride complexes with a mega-large stokes shift and unexpectedly high fluorescence quantum yield, *Chem. Commun.* 56 (14) (2020) 2159–2162.
- [52] G. Aquilanti, M. Giorgetti, M. Minicucci, G. Papini, M. Pellei, M. Tegoni, et al., A study on the coordinative versatility of new N,S-donor macrocyclic ligands: XAFS, and Cu<sup>2+</sup> complexation thermodynamics in solution, *J. Chem. Soc. Dalton Trans.* 40 (12) (2011) 2764–2777.
- [53] J.E. Hahn, R.A. Scott, K.O. Hodgson, S. Doniach, S.R. Desjardins, E.I. Solomon, Observation of an electric quadrupole transition in the X-ray absorption spectrum of a Cu(II) complex, *Chem. Phys. Lett.* 88 (6) (1982) 595–598.